Interactions of Excited Lithium Atom with Molecular Hydrogen. II. Properties of Wave Functions in the Potential Crossing Region

Kimiko MIZUTANI,* Takakazu YANO,† Atsushi SEKIGUCHI,†† Kazuko HAYASHI,††† and Shiro MATSUMOTO
Department of Chemistry, College of Science and Engineering, Aoyama Gakuin University, Chitosedai, Setagaya-ku, Tokyo 157
(Received January 31, 1984)

To elucidate the electronic mechanism of the quenching of electronically excited Li atoms by H_2 molecules, CASSCF calculations were made regarding the Li-H_2 system with various geometries. Special attention was payed to the electronic structure of the system in the crossing, or pseudocrossing, region of the potential energy surfaces. Simple CASSCF functions do not have a satisfactory spacial symmetry when the upper and the lower states are almost degenerate in energy, and need to be refined by the addition of a nonorthogonal CI. In the crossing region, electron density maps have shown that the Li atom is bonded more strongly to the nearer H atom than to the farther H atom in the ground state, whereas the opposite is the case for an excited state. Such properties of the wave function lead naturally to a picture of a nonadiabatic process occurring in the crossing region. The pseudocrossing of the first excited and the ground state potential energy surfaces has also been found for all geometries midway between the C_{2v} and $C_{\infty v}$ symmetries.

In a previous report,[1] we have shown that for the Li-H_2 system, the lowest $^2A_1$ and $^2B_2$ potential energy surfaces cross in a line located in an energetically accessible region. This has been determined as being the critical region where the nonadiabatic transition between an excited state and the ground state occurs with fair probability. However, the C_{2v} geometry seems to be too restrictive to describe the whole nonadiabatic process occurring in the system. It has thus become desired that the calculation be extended to more general geometries. Extensive calculations for the Li-H_2 system have been reported by P. J. A. Ruttink and J. H. van Lenthe,[2] and A. F. Wagner and A. C. Wahl[3] using large basis functions. Quite recently, Hobza and Schleyer[4] have reported calculations on the ground state of a Li-H_2 complex with MP2/6—311G (2d, 2p). These calculations, however, do not include any description concerning nonadiabatic transitions.

We report, in this paper, the results of further calculations using more general geometries[5] in order to search for other channels of the nonadiabatic transitions. The properties of the electronic wave function with regard to the geometries around the critical region were studied in some detail. The low-lying potential energy surfaces with a $C_{\infty v}$ geometry did not come close to each other. However pseudocrossing regions did exist for geometries intermediate between the C_{2v} and $C_{\infty v}$ symmetries, although they were located at somewhat higher energies. The MCSCF wave function, including insufficient CSF's, showed inappropriate properties in the critical region. The defect could be corrected by including an additional nonorthogonal configuration interaction.[11c] However, an examination of the crude wave functions led to a new schematic view of the nonadiabatic process. Meyer *et al.*[6] recently reported results of studies on the Na-H_2 system which were conducted for a similar reason as the one reported here. Our results for Li-H_2 parallel theirs in many respects.

Method of Calculation

Geometric parameters were taken as shown in Fig. 1. The bases were minimal STO-3G[7] functions, the electronic wave functions were computed with a CASSCF method,[8] and all orbitals other than the core orbital (1a′) were included in the active space. Computational details and notations are the same as those previously described.[1] The convergence of the MCSCF calculations was judged by the sum: $\sum_p \sum_{q(\neq p)} \langle\phi^p|\hat{R}|\phi^q\rangle^2$, as well as by the steadiness of the energy expectation values. In the above sum, ϕ^p denotes the p-th orbital function just computed, and $\hat{R}$ is the coupling operator.[1] Summations are taken over all the different pairs of orbitals. The value of the sum is denoted as the "residue" below, which should vanish at complete self-consistency. Iterations were continued until the residue value fell below 10^{-20} (hartree)^2. Good convergence was essential for assuring the quality of the wave functions. In one instance, a wave function with a residue value of 10^{-14} (hartree)^2 gave density maps that were quite different from those obtained from a wave function well converged to a residue value of less than 10^{-20} (hartree)^2.

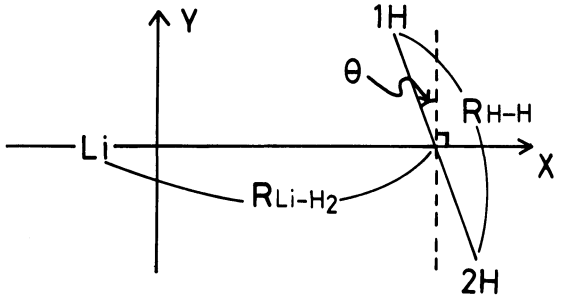

Fig. 1. Geometrical parameters for the Li-H_2 system.

†Present address: Citizen Watch Co., Tokorozawa, Saitama, 359.

††Present address: Anelva Corporation, Fuchu, Tokyo, 183.

†††Present address: Aoyama Gakuin High School, Shibuya-ku, Tokyo 150.

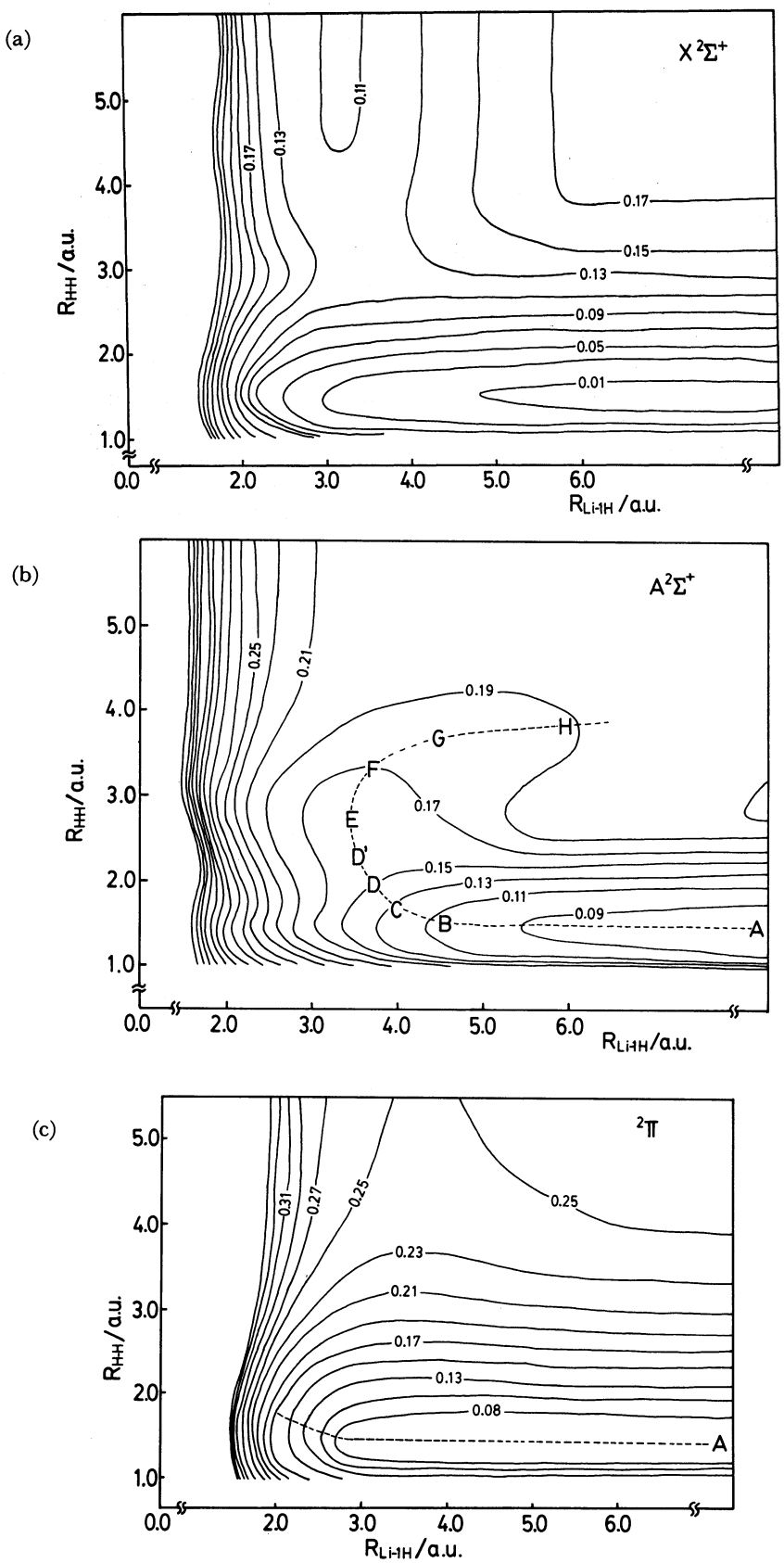

Fig. 2. Two-dimensional potential energy surfaces for the collinear geometry θ=90°; (a) X $^2\Sigma^+$, (b) A $^2\Sigma^+$, and (c) $^2\Pi$. Energies are given in hartrees minus −8.47 on each curve (dashed line is the minimum energy reaction path on the A $^2\Sigma^+$ surface and on the $^2\Pi$ surface, A, B, ···, H are several selected points on the curve).

Results and Discussion

Potential Energy Surfaces in $C_{\infty v}$ Geometry. Figure 2(a) shows the ground state potential energy surface. Figures 2(b) and 2(c) are the two excited state potential energy surfaces leading to a ground hydrogen and to the 2 ^{2}P lithium atom computed with $C_{\infty v}$ symmetry. It can be seen that neither of the excited potential energy surfaces come close to the ground state surface, unlike in the case with a C_{2v} geometry.[1] The minimum energy path, starting from isolated H_2 ($X\ ^1\Sigma_g$) and Li (2 ^{2}P) is shown by a dashed line on each excited state surface. The energy differences between the ground and the excited states along these lines are shown in Fig. 3. It seems, therefore, that a $C_{\infty v}$ geometry is far less favored for the quenching process of a 2 ^{2}P Li atom than the C_{2v} geometry,at least at moderate temperatures.

Potential Energy Surfaces for θ=45°. The ground and the first excited state potential energy surfaces for the arrangement θ=45° are shown in Fig. 4. Both states belong to the A′ representation of the C_s point group, and cannot intersect with each other. However, the surfaces come close together in the region shown by short dashed lines in Fig. 4. Figure 5 shows a cross section of the potential surfaces parallel to the ordinate. The potential curves display features of pseudocrossing. It is tempting, therefore, to speculate that nonadiabatic transitions may occur around these geometries, although their energies are somewhat higher than in the C_{2v} case.

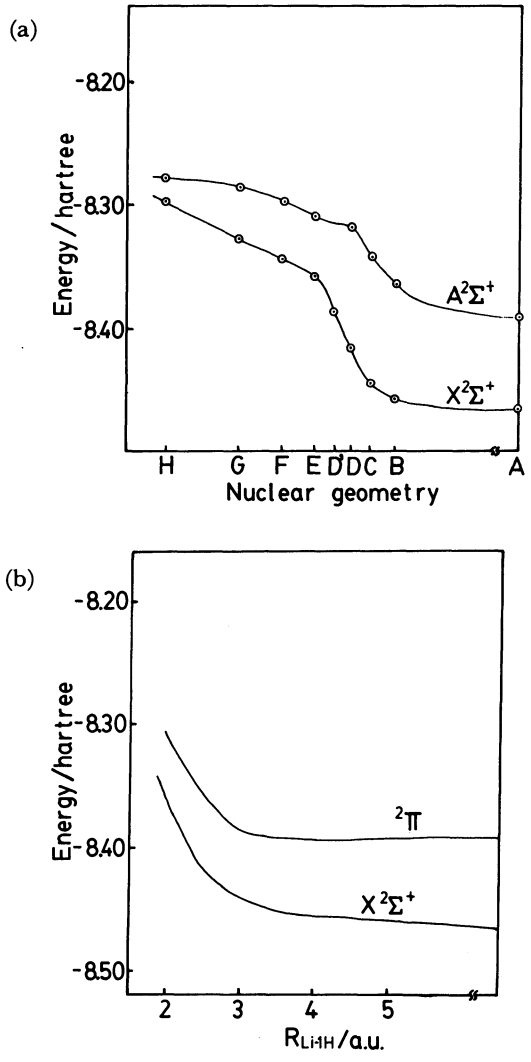

Fig. 3. Energies along the minimum energy path in Fig. 2(b) and 2(c), respectively; (a) $X\ ^2\Sigma^+$, $A\ ^2\Sigma^+$, and (b) $X\ ^2\Sigma^+$, $^2\Pi$. Nuclear geometries A, B, ···, H in Fig. 3(a) correspond to those in Fig. 2(b).

Properties of Potential Energy Surfaces Near the Critical Region of C_{2v} Potential Crossing. It is important to examine the wave function of the system for all the variations of nuclear geometry in the critical region in order to obtain a picture of the nonadiabatic process and to have an estimate of its occurrence probability. Even for the present simplest system, there are three degrees of freedom of the nuclei, and this is a nontrivial task. As an attempt, we selected "normal coordinates" around a geometrical point which seemed to be characteristic of the crossing (or pseudocrossing) region. The central point may be appropriately assigned to the lowest point (hereafter called "point P") on the intersection line of $^2B_2$ and $^2A_1$ surfaces (Figs. 2 and 3 of Ref. 1). By transforming the coordinate system ($R_{Li\text{-}H_2}$, $R_{H\text{-}H}$) to a mass-weighted system ($(m_{Li}\ m_{H_2}/(m_{Li}+m_{H_2}))^{1/2}\ R_{Li\text{-}H_2}$, $(m_H/2)^{1/2}\ R_{H\text{-}H}$), and by drawing a tangent and a normal at point P to the potential contour line passing through P, we obtained a type of normal coordinate system (Fig. 6). We had, of course, two different coordinate systems depending on which of the potential surfaces we utilized. In practice, the two sets of directions turned out to be not very different, and we took the one constructed on the $^2B_2$ surface, as we expected the process to be occurring from the excited state. Calculations with a larger basis sets[9] revealed the same feature. We shall call the normal direction as the reaction coordinate and the tangential direction as the direction of C_{2v} vibration, for convenience. Another vibrational degree of freedom is an antisymmetric stretching mode (b_2) analogous to that of a stable isosceles triangular molecule. It coincides to the first order with a θ-deformation (*i.e.* rotation by θ (Fig.1) of the H_2 molecule about its center while the center and the inter-hydrogen distance are fixed). Thus, we have taken the angle θ as the third parameter describing the nuclear geometry for visual simplicity and for later conveniences of discussing rotational perturbation separately. The normal vibration of the C_{2v} symmetry plays a role which becomes important only for more quantitative calculations of transition probabilities. Thus, we defer its inclusion until the results of more quantitative calculations are discussed. Figure 7 shows potential energy curves for a θ-deformation at point P,[10] and at several points along the reaction coordinate. The potential curve at P consists virtually of two quasiparabolas crossing at P and symmetrically placed

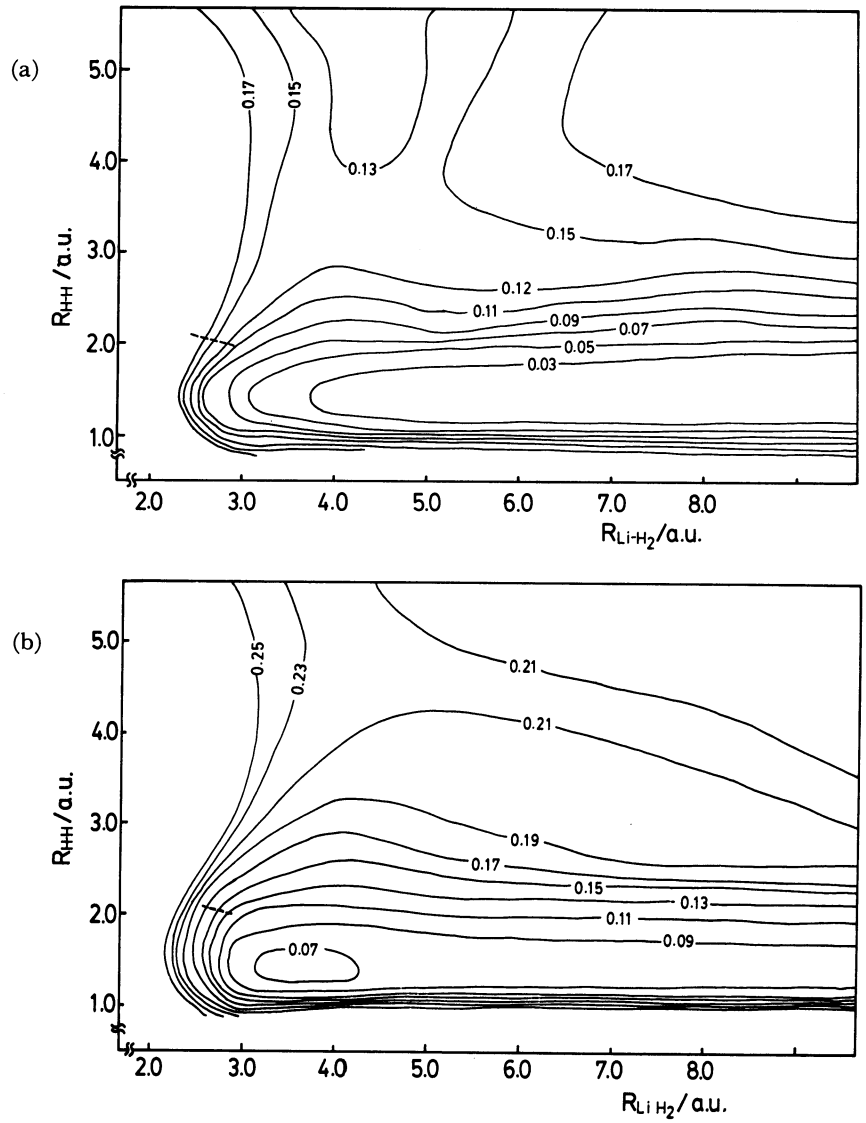

Fig. 4. Potential energy surfaces for C_s geometry θ=45°; (a) lowest $^2A'$ and (b) 2nd. $^2A'$. Energies are given in hartrees minus −8.47 on each curve.

with respect to the ordinate. The points of energy minima lie only slightly lower than P, but they are distinctly displaced from the ordinate. The ground state potential energy curves at points on the reaction coordinate other than P have similar minima, while each of their excited counterparts has a single minimum at θ=0°. It will be noticed that while the ground state potential energy curves at Q''' and R''' have cusps at θ=0°, other ground state curves passing through points more distant from P look smooth at θ=0°. This fact is related to with the quality of our MCSCF wave functions and will be discussed in the next section.

Singularity of MCSCF Wave Functions in a Critical Region. The electron density maps of the 3a′ natural orbitals of the two (nearly)[10] degenerate MCSCF wave functions at point P were obtained by CASSCF calculations and are shown in Fig. 8. As may be apparent from the figures, these two wave functions are in themselves neither symmetric nor antisymmetric with respect to the xz-plane, but are mutually symmetric with respect to this plane, in contradiction to group theoretical requirements. The mirror image relationship is also seen in the 1a′ core orbitals of both wave functions (Tables 1 and 2). A similar dissymmetry of the wave functions is observed when the ground state potential energy curves display cusps, as shown in Fig. 7. In separate CASSCF calculations we obtained MCSCF wave functions while constraining the orbitals to belong to irreducible representations of the C_{2v} point group. The energies of the resulting two wave functions ($^2A_1$ and $^2B_2$) again agreed to 10^{-9} hartree, but were somewhat higher than those without the symmetry constraints on the orbitals. These phenomena have resulted from the near degeneracy of the 3a′ and 4a′ orbitals[11c] and/or the imperfectness of the CSF's involved in the calculation. They may be of the same sort as the doublet instability[11] found for

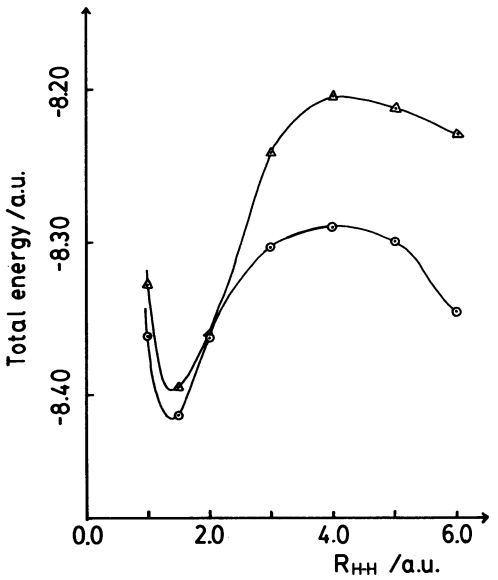

Fig. 5. A cross section of the potential energy surfaces of Fig. 4 cut by a plane perpendicular to the sheet and parallel to and apart by 3.0 bohr from ordinate. ⊙: lowest $^2A'$, ▲: 2nd. $^2A'$.

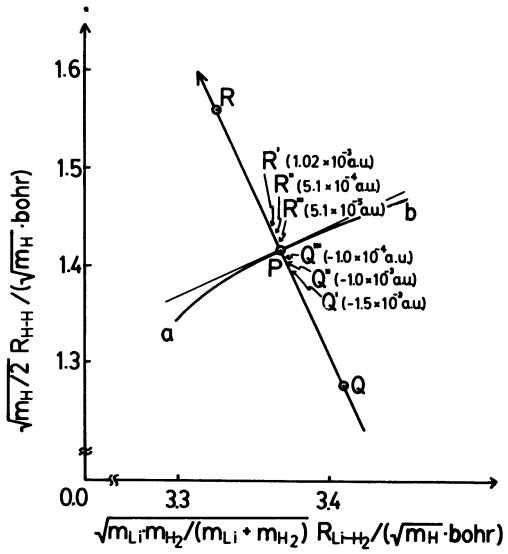

Fig. 6. Normal coordinate system at the lowest point P of the crossing seam of the lowest $^2A_1$ and $^2B_2$ surfaces, displayed in mass weighted scale. aPb is the energy contour line through P and QPR corresponds to the reaction coordinate on the $^2B_2$ surface. The figures beside letters R', R'', *etc.* are the distances from point P.

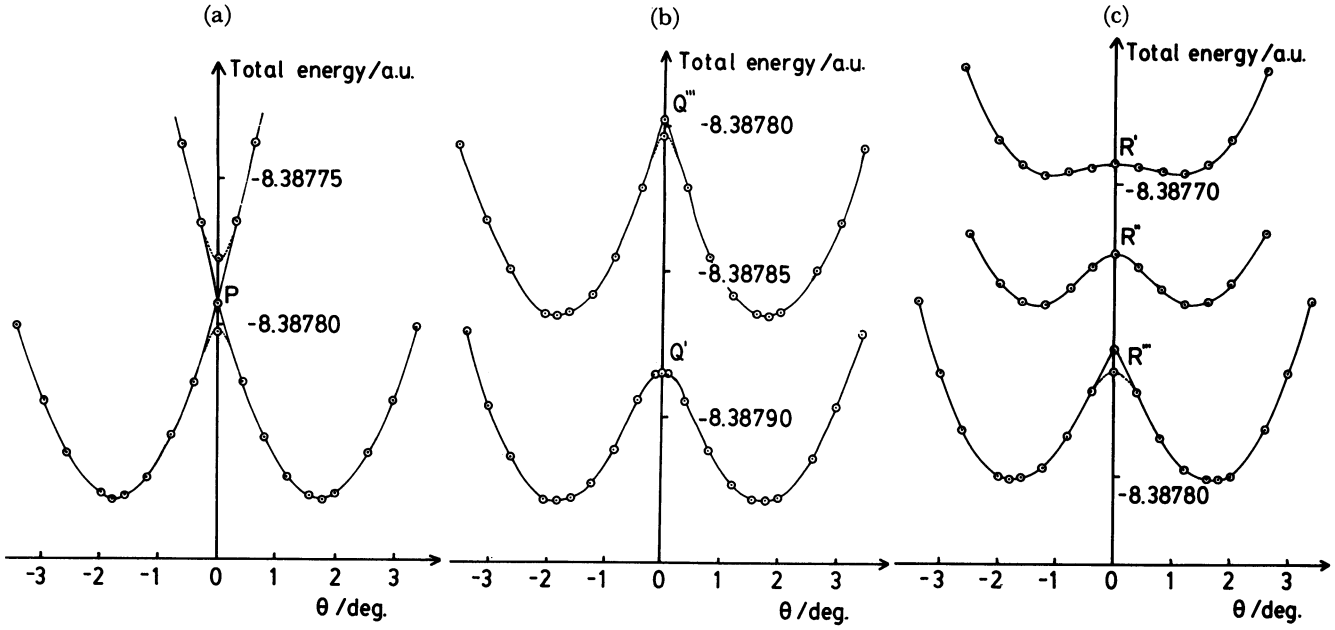

Fig. 7. Total energy *versus* C_s deformation angle from C_{2v} geometry passing: (a) P, (b) Q', and Q''', and (c) R', R'', R'''. The locations of P, Q', Q''', R', R'', and R''', are shown in Fig. 6. In (b) and (c), only the lower state curves are shown. As to the dashed curves see text.

some stable molecules. Thus, MCSCF wave functions composed of only limited CSF's should be handled with care near geometries where potential crossing occurs, though those functions are quite good in other regions as will be shown below. One remedy is to perform an additional nonorthogonal CI[11c] between the wave functions. Thus, at P two wave functions are obtained, each belonging to one of the irreducible representations of the symmetry point group. The results of this treatment are shown in Fig. 9 and by dashed lines in Fig. 7(a). The energy displacements were of the order of 10^{-6} hartree at point P. Thus, the two curves crossing at P separate out into two smooth pseudocrossing curves. The same smoothing out of the potential curves passing through Q''' and R''' is shown in Fig. 7 as dashed lines. It will be noted, from the figure, that though the singularity is marked, qualitatively, it is relatively insignificant, quantitatively. Energy shifts resulting from the additional nonorthogonal CI are only remarkable (though the actual values are quite small) near the degenerate point, and do not alter the gross appearance of the MCSCF potential surfaces. The insignificance of the additional CI outside the critical region is seen from the data shown in Table 3.

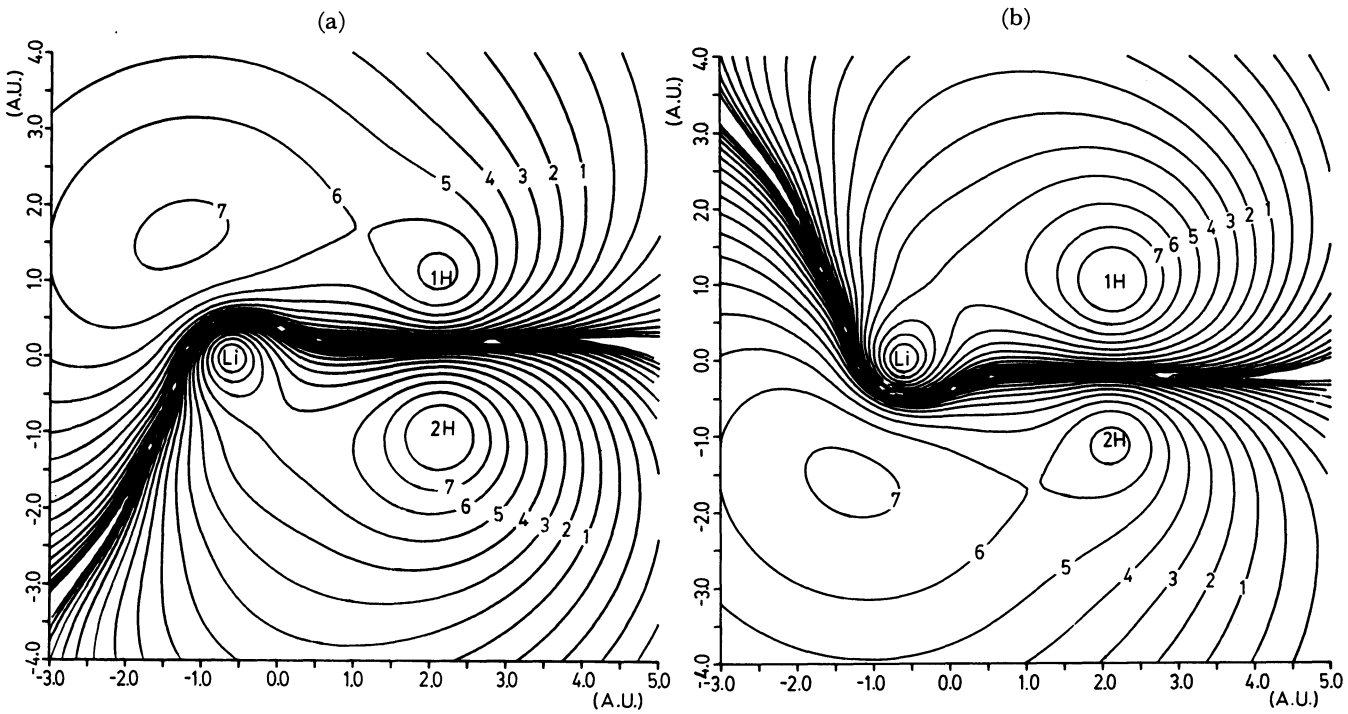

Fig. 8. Contour plots of 3a′ natural orbital electron density of simple MCSCF functions at P; each of (a) and (b) displays either one of the mutually symmetric pair functions degenerate at P. They correspond two states shown by the two curves in Fig. 7(a). The numbers 1, 2, ···, and 7 beside the contours indicate electron density of 3.5565×10^{-4}, 6.3246×10^{-4}, 1.1247×10^{-3}, 2.000×10^{-3}, 3.5565×10^{-3}, 6.3246×10^{-3}, 1.1247×10^{-2} electrons/bohr^3, respectively.

Table 1. Natural orbitals of one of the wave functions degenerate at point P

Basis	MO	$\phi_{1a'}$	$\phi_{2a'}$	$\phi_{3a'}$	$\phi_{4a'}$
Li	1s	0.9956	−0.1087	−0.1069	0.0567
Li	2s	0.0216	0.0931	0.6076	−0.3182
Li	$2p_x$	−0.0036	0.1039	−0.2871	0.1676
Li	$2p_y$	0.0022	0.0076	−0.6304	0.3310
1H	1s	0.0030	0.5329	−0.3180	−0.9401
2H	1s	0.0022	0.5111	0.1835	1.0163

Table 2. Natural orbitals of the other wave function of the degenerate states at point P

Basis	MO	$\phi_{1a'}$	$\phi_{2a'}$	$\phi_{3a'}$	$\phi_{4a'}$
Li	1s	0.9956	−0.1087	−0.1069	0.0567
Li	2s	0.0216	0.0931	0.6076	−0.3182
Li	$2p_x$	−0.0036	0.1039	−0.2871	0.1676
Li	$2p_y$	−0.0022	−0.0076	0.6304	−0.3310
1H	1s	0.0022	0.5111	0.1835	1.0163
2H	1s	0.0030	0.5329	−0.3180	−0.9401

Full CI calculations are also feasible with the small basis set used here. Preliminary results of the full CI calculation[12] closely parallel those of the above CI-corrected functions.

Bond Exchange View of the Nonadiabatic Transition. The "primitive MCSCF function" shown in Figs. 7(a) and 8 have certain defects. They are, however, illustrative of an important property of the adiabatic function near the crossing. The electronic wave function should belong to one of the representations of the C_{2v} point group when the nuclear arrangement has that symmetry. It is more properly described as a linear combination of two mutually symmetric components having the features shown in Fig. 8, rather than by a single one of them. As the nuclear geometry is deformed by a very small angle θ[13] from a precise isosceles structure, one of the components rapidly reveals its predominance, as is be apparent from the small separation of the dashed lines from the solid lines in Fig. 7(a). For example, when θ is slightly positive, the electronic structure is characterized by a 3a′ natural orbital closely resembling that in Fig. 8(a). The 3a′ orbital bonds Li more strongly to the nearer 1H than to the farther 2H, and forces the geometry farther to the potential minima at a positive θ value. The feature of the corresponding excited state in this situation is characterized by the 3a′ natural orbital essentially of the form of Fig. 8(b). In this state, the distant 2H atom is more strongly bonded to the Li than the nearer 1H. In this sense, the nonadiabatic transition near point P may be viewed as a bond-type change, which occurs smoothly. It is noted that the potential curves in Fig. 7(a) (and more schematically in Fig. 10) are similar to those used to schematize a bimolecular replacement reaction.[14]

A rapid change in the mixing coefficients of the wave functions of the type represented in Fig. 8(a) and those in Fig. 8(b) as we pass through $\theta=0°$ means there is a strong dependence of the wave function on the nuclear geometry. That is a condition[15] which is necessary for the electronic transitions caused by nuclear motion. More specifically, we can view each single state of Fig. 7(a) as a kind of diabatic state[16] appropriate to describing the nonadiabatic transition at P (or its

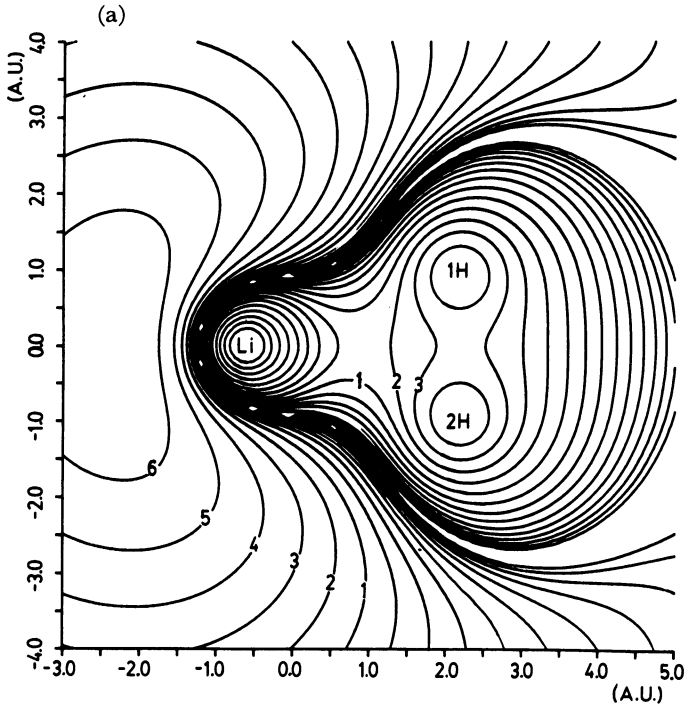

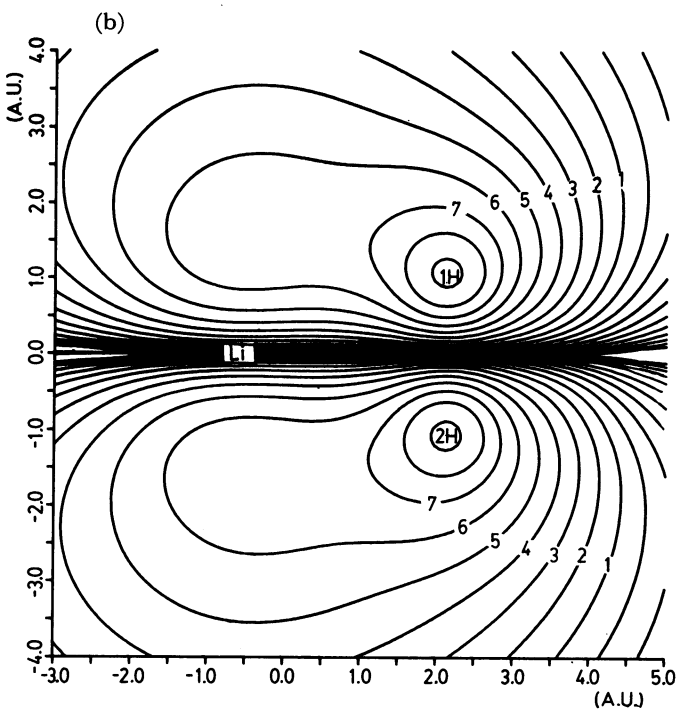

Fig. 9. Contour plots of 3a′ natural orbital electron density of wave functions at P, corrected by an additional CI; (a) upper state and (b) lower state. Figures besides contours have the same meaning as in Fig. 8.

Table 3. Energy difference and energy shifts after an additional nonorthogonal CI

$E_2^0-E_1^{0a)}$	$<1.0\times10^{-10}$	7.4×10^{-5}	7.9×10^{-3}	4.3×10^{-2}
$\lvert\Delta E_1\rvert$	5.8×10^{-6}	1.6×10^{-7}	8.5×10^{-10}	$<1.0\times10^{-15}$
$\lvert\Delta E_2\rvert$	7.6×10^{-6}	1.3×10^{-7}	3.5×10^{-9}	$<1.0\times10^{-15}$

a) Energy difference between the excited $^2A'$ state and the ground $^2A'$ state before an additional CI. Energy unit is hartree.

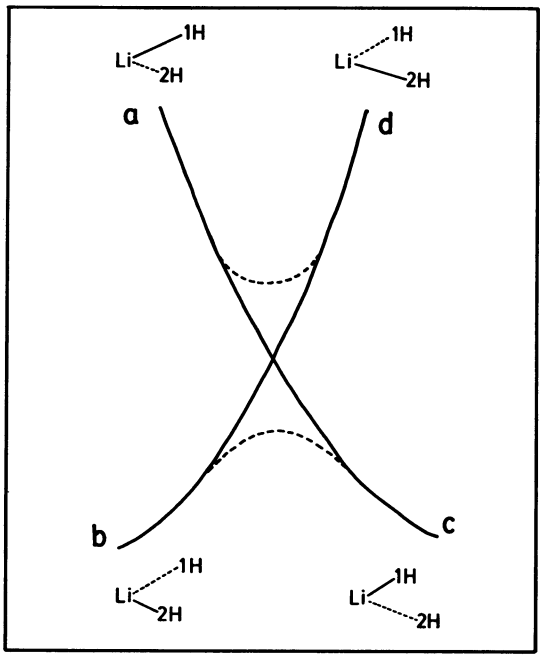

Fig. 10. Schematic representation of potential curves in the pseudocrossing region.

neighborhood) caused by a θ vibration.[11c] Thus as θ changes from a negative to a positive value with a finite velocity, there is a finite probability that the state of the system will follow the diabatic curve from *a* to *c* rather than the adiabatic curve (dashed line) from *a* to *d* (Fig. 10). In other words, there is a finite probability that the system changes from a state in which a more distant atom pair is bonded to a state of the inverse bonding mode.

The presence of cusps in the potential curve at $\theta=0°$ (Fig. 7) is related to the singularity of the density map at $\theta=0°$. The density maps of the 3a′ natural orbitals for points Q', R', and R'', where virtually no cusps are discernible, have a C_{2v} symmetry, while those for points Q''' and R''' have more or less similar abnormal features found at P. We made careful calculations at numerous points along the reaction coordinate and found that the change from the normal behaivor at points far from P to the abnormal one near P was, in reality, continuous. Moreover, the same series of converging functions were obtained irrespective of the starting 0-th approximation of the wave function. Thus, it seems that the singularity seen in the wave function obtained at P and its neighborhood was not the result of pathological progressions of iterations, but the result of an inappropriate form of wave function, as noted above.

Figure 11 shows the potential energy contour maps, thus computed, on the QR-θ plane. Figure 12 is a wide view comprising θ values up to 90°. It shoud be noticed that the shallow channels located at both sides of the reaction coordinate in Fig. 11 are quite immaterial in the gross potential surface (Fig. 12). The depth of the channels was only of the order of

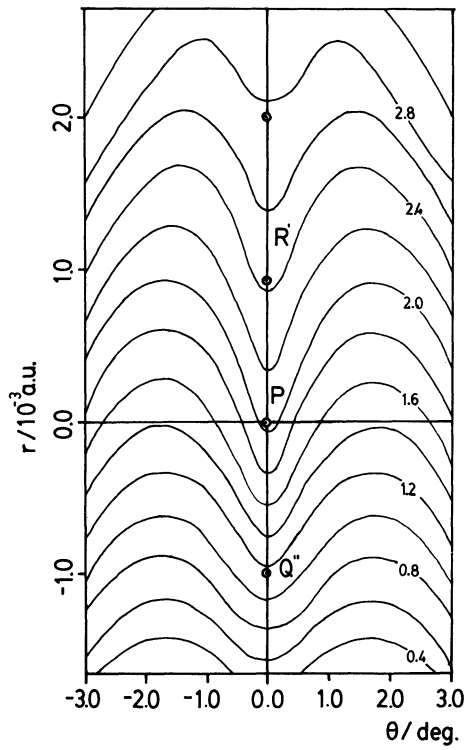

Fig. 11. Contour plots of the potential energy surface of the lowest $^2A'$ state near point P for C_s deformation (finer view). Abscisa: angle of deformation from C_{2v}. Ordinate: reaction coordinate. Figures beside curves indicate the values (E_{total}+8.3880 hartrees)/(10^{-4} hartree).

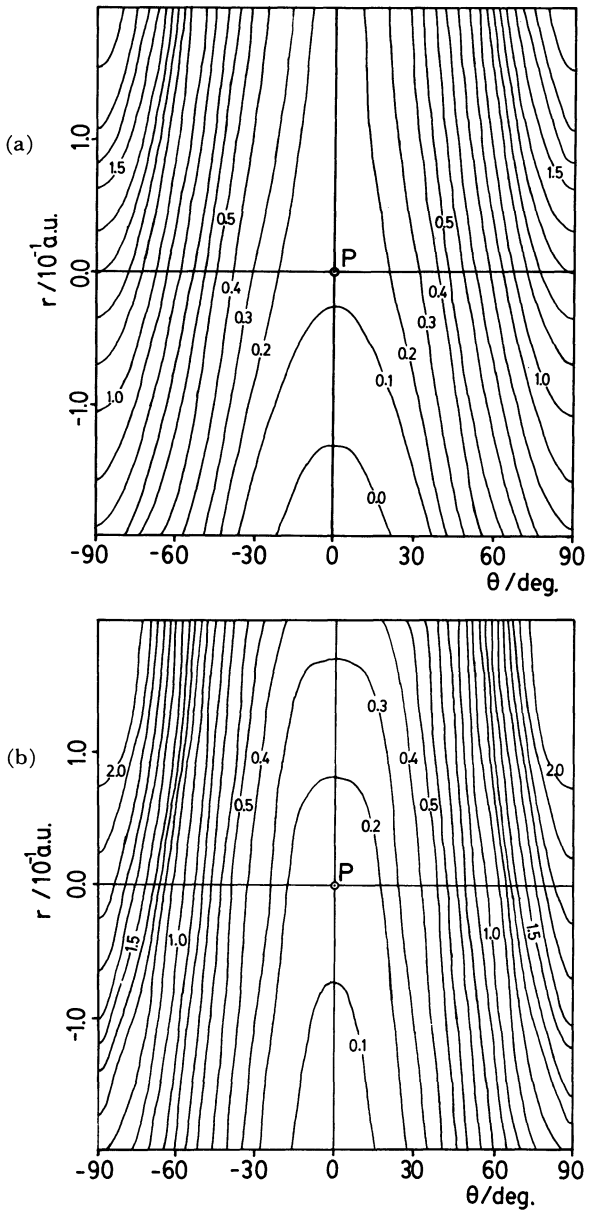

Fig. 12. Contour plots of the potential energy surfaces of the two lowest $^2A'$ states for C_s deformation from C_{2v}. (wider view). Abscisa: deformation angle from C_{2v}. Ordinate: reaction coordinate. (a) lowest $^2A'$ and (b) 2nd. $^2A'$. Figures beside curves indicate the values (E_{total}+8.4000 hartree)/(10^{-1} hartree).

50cal/mol in this calculation. It may be neglected compared to thermal energy in the usual quenching experiments. The steep ascent of the potential surface to the θ direction implies the energetic disadvantages of a transition through a skewd geometry, as described at the beginning of this discussion. It is interesting that even for linear arrangement of the nuclei, the 3a' natural orbital shows similar bond exchange features as found above for the nearly C_{2v} geometry. Figure 13 shows electron density maps at point F of Fig. 2, and is compared with features shown in Figs. 8 and 9. The whole view of the first and second potential energy surfaces displayed with R_{LiH_2} and θ as parameters may be sketched roughly as in Fig. 14. They touch conically near point P in this dimension.

Conclusions

Potential energy surfaces of a system consisting of an $X^1\Sigma_g^+H_2$ and a Li atom in either 2^2S or 2^2P state come close or even cross, aside from collinear arrangement, for almost all inclination angles of the H_2 axis relative to the direction joining the components. Quenching of the excited Li atom by the H_2 molecule is expected to occur along any of the paths passing through these crossing regions. Among these paths, the ones having an isosceles or nearly isosceles geometry seem to be energetically most favorable. CASSCF wave functions,in which all the orbitals other than the core are included as active states, are almost as good as the full CI wave functions for every nuclear geometry in describing the finer electron density profiles as well as the energetic behavior of the system, except for small cririca regions where crossing or pseudocrossing occur. In the latter regions it is necessary to perform an additional nonorthogonal configuration interaction, or full CI if possible. Energetic corrections are quite small in these regions. The primary wave functions, themselves, reveal characteristic electronic properties of the system in the crossing region. Around the pseudocrossing point, ground state potential curves for

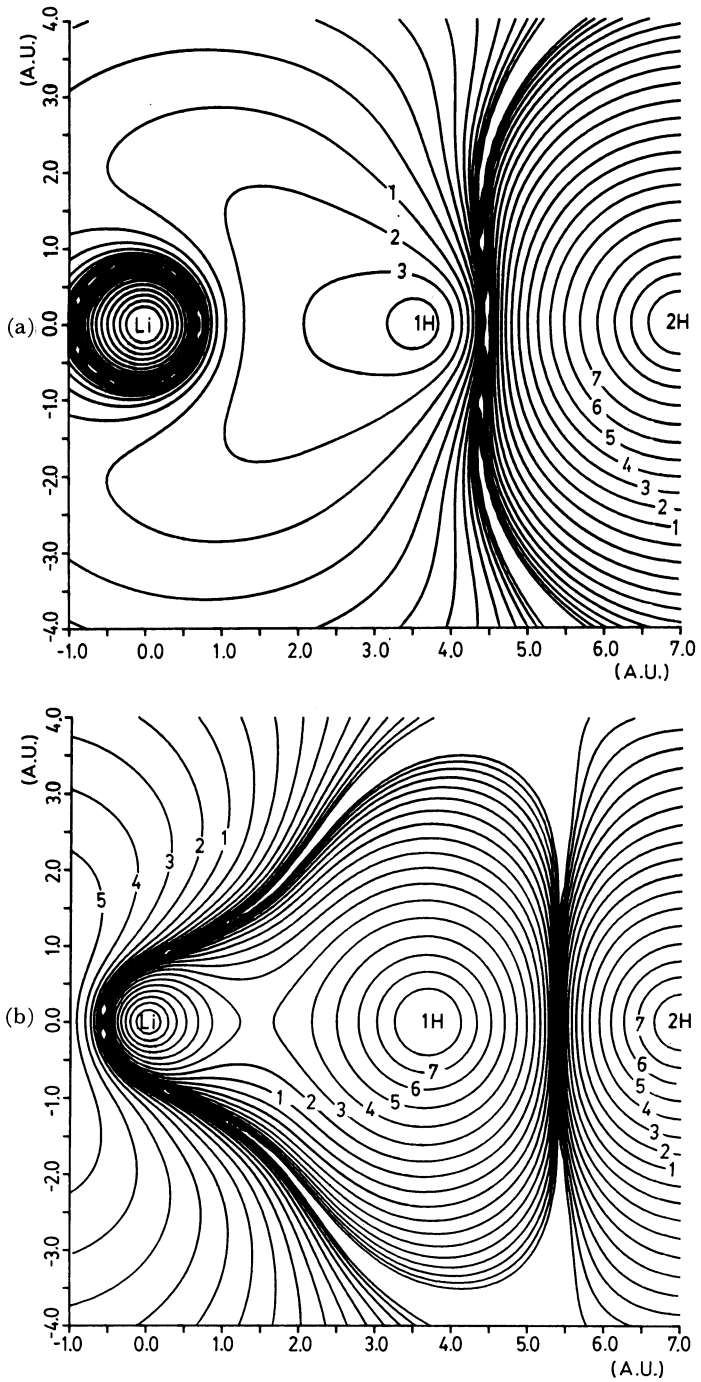

Fig. 13. Contour plots of 3a′ natural orbital electron density map for collinear geometry θ=90°, $R_{Li\text{-}H_2}$= 3.7 bohr, $R_{H\text{-}H}$=3.3 bohr. (a) lowest $^2\Sigma^+$ and (b) 2nd. $^2\Sigma^+$. Figures beside curves have the same meaning as in Fig. 8.

a θ-deformation from the C_{2v} geometry have shallow but distinct minima located at a few degrees on both sides. The whole potential curves may be viewed as resulting from a resonance splitting of the two crude "diabatic" curves, each describing one of the two modes of bonding. In this connection, electron density maps reveal features of bond type alternation upon nonadiabatic transitions induced by the b_2 vibration of the complex. These features resemble the mechanism of a bimolecular exchange reaction.

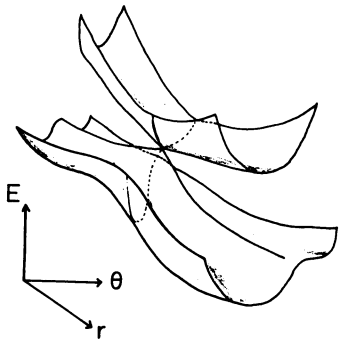

Fig. 14. Schematic view of the $1^2A'$ and the $2^2A'$ adiabatic potential energy surfaces in θ and r dimensions near the conical touch points.

We thank Professor Keiji Morokuma and Dr. Shigeki Kato of the Institute for Molecular Science for their helpfull suggestions, discussions and encouragement. Calculations were carried out at the Computer Center of the IMS, Okazaki National Research Institutes, at the Computer Center of the University of Tokyo, and at the Aoyama Gakuin University Computer Center. Thanks are due to Mr. Toyama for his help in these calculations. The present work was partially supported by a Grant-in-Aid for Scientific research No. 57740248 from the Ministry of Education, Science and Culture.

References

1) K. Mizutani, Y. Kuribara, K. Hayashi, and S. Matsumoto, *Bull. Chem. Soc. Jpn.*, **52**, 2184 (1979).

2) P. J. A. Ruttink and J. H. van Lenthe, *Theor. Chim. Acta.*, **44**, 97 (1977).

3) A. F. Wagner, A. C. Wahl, A. M. Karo anfd R. Krejci, *J. Chem. Phys.*, **69**, 3756 (1978).

4) P. Hobza and P. R. Schleyer, *Chem. Phys. Lett.*, **105**, 630 (1984).

5) Part of the results was presented by K. Hayashi, K. Mizutani, and S. Matsumoto at the 41st. National Meeting of the Chemical Society of Japan, Osaka, April 1980, Abstr. P. 170.

6) P. Botschwina, W. Meyer, I. V. Hertel, and W. Reiland, *J. Chem. Phys.*, **75**, 5438 (1981).

7) W. J. Hehre, R. F. Stewart and J. A. Pople, *J. Chem. Phys.*, **51**, 2657 (1969).

8) B. O. Roos, P. R. Taylor and P. E. M. Siegbahn, *Chem. Phys.*, **48**, 157 (1980); P. E. M. Siegbahn, J. Almlof, A. Heiberg and B. O. Roos, *J. Chem. Phys.*, **74**, 2384 (1981).

9) Given at Molecular Structure Symposium, October 1981, Kyoto, Japan, Abstr. No. 2M02 and will be published separated paper.

10) At point P, the energies of $^2A_1$ and $^2B_2$ states almost coincide (to 10^{-10} hartree in this case). However, after an additional CI (see below), it is no more a point of potential surface intersection. Actually, it was a point somewhat displaced toward point R in Fig. 6 after the nonorthogonal CI.

11) a) J. Paldus and J. Cizek, *Chem. Phys. Lett.*, **3**, 1 (1969); J. Paldus and J. Cizek, *J. Chem. Phys.* **52**, 2919 (1970); b) A.

Toyota and T. Nakajima, *Bull. Chem. Soc. Jpn.*, **50**, 97 (1977); c) C. F. Jackels and E. R. Davidson, *J. Chem. Phys.*, **64**, 2908 (1976).

12) Given at the 49th National Meeting of the Chemical Society of Japan, Tokyo, April 1984, Abstr. p. 38.

13) Calculations showed that only an order of 5×10^{-2} degree deformation was sufficient.

14) S. G. Christov, "Lecture Notes in Chemistry, 18, Collision Theory and Statistical Theory of Chemical Reactions," Springer-Verlag, Berlin, 1980, p. 19.

15) T. F. O'Malley, "Advances in Atomic and Molecular Physics Vol. 7" Academic Press, New York, 1971, p. 227; E. E. Nikitin and L. Zulicke, "Lecture Notes in Chemistry, 8, Theory of Chemical Elementary Processes," Springer-Verlag, Berlin, 1978, p. 20.

16) T. F. O'Malley, "Advances in Atomic and Molecular Physics Vol. 7," Academic Press, New York, 1971, p. 223; R. Cimiraglia and M. Persico, *Mol. Phys.*, **38**, 1707 (1979).